metals

MDPI

Review

Computational Methods for Lifetime Prediction of Metallic Components under High-Temperature Fatigue

Vitaliy Kindrachuk *, Bernard Fedelich, Birgit Rehmer and Frauke Peter

Federal Institute for Materials Research and Testing (BAM), Unter den Eichen 87, 12205 Berlin, Germany; bernard.fedelich@bam.de (B.F.); birgit.rehmer@bam.de (B.R.); fraukepeter@web.de (F.P.)

* Correspondence: vitaliy.kindrachuk@bam.de; Tel.: +49-30-8104-4352

Received: 19 February 2019; Accepted: 21 March 2019; Published: 28 March 2019

Abstract: The issue of service life prediction of hot metallic components subjected to cyclic loadings is addressed. Two classes of lifetime models are considered, namely, the incremental lifetime rules and the parametric models governed by the fracture mechanics concept. Examples of application to an austenitic cast iron are presented. In addition, computational techniques to accelerate the time integration of the incremental models throughout the fatigue loading history are discussed. They efficiently solve problems where a stabilized response of a component is not observed, for example due to the plastic strain which is no longer completely reversed and accumulates throughout the fatigue history. The performance of such an accelerated integration technique is demonstrated for a finite element simulation of a viscoplastic solid under repeating loading–unloading cycles.

Keywords: fatigue; incremental lifetime models; finite element analysis

1. Introduction

Performance of metallic components subjected to high temperatures is of primary concern in the design and reliability analysis of engines, power plants, etc. The engineering interest in their safe service has risen in the last century due to permanently increasing temperature range, whereas the focus of materials science is on understanding the primary damage mechanisms limiting the lifetime. One crucial example is the use of gas turbines for a variety of purposes including power generation [1], compression or as jet engines in aircraft [2]. Reliability of the gas turbines is a vital issue for safety aspects, in particular for safety of aircraft flights. The critical components of a gas turbine are the discs and the high-pressure turbine blades [3], which operate under severe conditions. In addition to high temperatures, these include oxidation and mechanical loadings due to the centrifugal force, pressure of gas jet and vibrations. Therefore, the most advanced technologies are used for expensive manufacturing of such blades, especially for those which are solidified as single-crystals of Ni-based superalloys in order to withstand the severe loading conditions [4]. Nevertheless, the time in service of the discs and blades is limited because of raising risk of failure. This is often caused by vibration-induced fatigue and thermo-mechanical fatigue (TMF) which is attributed to the thermal cycles consisting in the starts and stops of a turbine, e.g., taking off and landing of an aircraft.

TMF also occurs in other sectors of industry [5]. Thus the current requirements for flexible power plants in order to compensate the fluctuations of the regenerative energy sources mean a significant increase in the number of start-ups and shut-downs, which leads to earlier damage in the heat exchangers. Another example concerns the hot components of a combustion engine. The turbocharger experiences slowly varying thermal loadings and high frequent pressure changes due to the repetitive

ignition process. Here, like in all combustion processes, the requirement of high thermodynamic efficiency implies higher service temperatures. This in turn promotes material ageing and creep strain accumulation, which subsequently enhance TMF. Fatigue is also known to be the main origin of failure in electronics components, temperature fluctuations result in stress reversals attributed to the thermal expansion mismatch between the different materials of the assembly and ultimately cause solder joint delamination [6]. The main challenge in the research of the mentioned fatigue failures is understanding the factors which influence the fatigue resistance, including the superposition of loadings and loading histories on the one hand, and the complex interaction of the resulting damaging mechanisms on the other hand. In particular for the metallic components, the prevalent damage mechanisms are fatigue, creep and oxidation. It is difficult to estimate the effect of the mentioned factors using only testing techniques. Furthermore, failure due to cyclic loads is generally not instantaneous, but characterized by a steady damage accumulation and may depend on the loading history. Therefore, the development of reliable models and computational techniques to predict the fatigue lifetimes of hot components is a key task in computational mechanics.

With the purpose to understand the requirements to lifetime models, it is useful to gain an insight into the particularities of macroscopic cyclic strain behavior. This falls in three following regimes: elastic shakedown, plastic shakedown and ratcheting. The elastic shakedown occurs if the plastic strains remain constant after a few cycles and the response becomes purely elastic. This regime is rather unusual with regards to the high temperature service. The plastic shakedown is the periodic in-time inelastic behavior that occurs once the so called stabilized cycle is reached. The material then experiences reversed plastic straining with no net directional accumulation of plastic deformation. This is in contrast to ratcheting in which the material accumulates a plastic strain during each cycle. The situations in which the last two regimes occur are common for metallic components subjected to high temperatures and belong to the scope of low-cycle (LCF) and thermo-mechanical fatigue. For industrial components, ratcheting must be prevented in the design and assessment phase, as accumulated plastic deformations would lead to a rapid failure of the structure. The plastic shakedown is therefore, the regime which is relevant for majority of practical applications. As a consequence, the most lifetime models predict the component time in service based on the assumption that the stabilized response exists.

A large number of sophisticated fatigue life criteria have been proposed, which bear on the parameters of the stabilized cycle. They are often referred to as parametric lifetime models. Examples are well known from the literature: models based on plastic or plastic and creep strains (Coffin–Manson, Solomon, Syed), stress-based (Basquin, Goodman, Walker) and energy-based models calculating the overall stress-strain hysteresis energy (Dasgupta, Pan, Benoit). The description and review of these and familiar parametric models can be found in [7–10]. Their in-depth discussion remains out of the focus of this paper. It is sufficient to mention that these models assume discrete evolution of damage from cycle to cycle, which is controlled by the respective integral parameters of the cycle. Another class of models assume a continuous damage evolution during each cycle. This evolution is formulated as an additional ordinary differential equation (ODE) with respect to the internal variable for damage. The advantage of this procedure is that it can be easily applied to compute the accumulation of damage throughout an arbitrary complex loading path and fatigue loading history. The technique can efficiently evaluate the intricate stress states, including non-proportional multiaxial loadings, unloadings and stress redistributions which can locally arise in the hot components. Doing so, the time scale is divided into small increments where the ODEs are evaluated and the changes of damage and other history variables are subsequently computed within each increment. Because of this integration procedure, the respective models based on the ODEs in time are denoted as incremental lifetime models. Nowadays, when the finite element simulations have become an established computational tool, the use of incremental approaches, in particular in the post processing analysis, is a straightforward procedure.

The mentioned methods are especially efficient for those simulations that early manifest the stabilized behavior. It is because the loading cycles result in the same lifetime consumption ΔD_s under

the stabilized response, so that the overall life span can be approximated by taking the inverse of the damage $N_f \approx \frac{1}{\Delta D_s}$. The stabilized behavior is possible if the damage evolution does not noticeably influence the macroscopic deformation behavior. This is the case if the component does not contain severe stress raisers or notches. The size of fatigue cracks usually ranges within the microscale, which is sufficiently small with respect to the dimensions of the regions where the macroscopic inelastic deformation occurs and with respect to the dimensions of the component itself. This is a common procedure in the engineering fatigue life assessment, while notches and joints are treated separately by heuristic corrections [11]. Once the evolution of damage affects the deformation behavior, in general by reducing the material stiffness [12], the stabilized response does not longer exist. An unsaturated response can be attributed to other reasons, for instance to unbalanced loading or simply to complex geometry of the component. The computational analysis becomes complicated, since the mechanic behavior is accompanied by softening. It promotes, in turn, the flow rate and localization of the inelastic strains and damage. Using a continuum mechanics framework for lifetime prediction in such situations requires numerical integration of evolving damage and other state variables until the onset of failure. This is however intractable in the engineering practice because of dramatical numerical expenses expected to integrate the whole fatigue loading history, which is in the order of 10^3–10^7 cycles. The challenge can only be overcome by the application of multiscale methods in space, like sub-modeling approach [13,14], and time. The latter rely on the extrapolation techniques, the so called cycle jump procedure, in order to approximate the fatigue loading history while keeping the numerical costs considerably low [15]. Note that using the accelerated integration methods in time can also be profitable for integration of the loading history until the stabilized response, if this appears after too many loading cycles.

The current paper considers first the incremental lifetime models. The widely used constitutive models of Chaboche [16] for polycrystals and of Cailletaud [17] for face-centered cubic (fcc) single crystals are presented as the essential parts of the incremental approaches. The method is applied to an austenitic cast iron under LCF and TMF conditions. Further, a parametric lifetime model will be discussed, which is based on the fracture mechanics concept. It operates with the crack tip-opening displacement while assuming a smooth geometry. Its ability to predict the lifetime of the same austenitic alloy is demonstrated for comparison goals. In our opinion, these examples cover the majority of situations where the parametric and incremental models are computationally advantageous. The focus is set on two damage mechanisms, namely due to fatigue and creep, whereas the consideration of the oxidation enhanced deterioration remains beyond the scope. In the final part, the current state of the research in the multiscale modeling in time is provided including the example for a coupled creep-damage interaction. It results in an unsaturated response and stress redistribution, which can be well treated by the cycle jump method.

2. Incremental Lifetime Models

The lifetime of a component ends with appearance of the technical crack(s) with the order of size of few millimeters. The cracks originate from growth and coalescence of the microcracks which generally initiate under cyclic loading on material imperfections (voids, pores), oxide spikes, precipitates, interfaces of the persistent slip bands or dislocation pile-ups on the surface (grain boundaries) [18,19]. The nucleation kinetics and the propagation rate of the microcracks are primary governed by the local deformation and stress states. Their description requires thus a proper constitutive modeling of the material response. This replaces the discrete flaws, microcracks etc. by the evolution of a damage variable leading to failure. As a consequence, an incremental lifetime approach consists of two parts: a viscoplastic continuum model to capture the inelastic deformation over the entire stress-temperature field and an incremental lifetime rule which suggests the damage evolution equation based on the local values of stresses an strains. The lifetime consumption is computed due to incremental time integration along the loading path, so that the damaging impact of any loading state is evaluated and contributes to the damage variable. This is advantageous against the conventional parametric

methods, since complex loading histories including creep-fatigue interaction can be evaluated, whereas an arbitrary partition of the strain in an instantaneous and a creep component is no longer necessary.

2.1. Deformation Models

In spite of a wide variety of constitutive models to simulate the inelastic deformation in the metallic component, the goal here is rather to provide the basics necessary for the further discussion of the lifetime rules. An appropriate constitutive model should reproduce the hardening behavior and the viscoplastic response which is crucial at high-temperatures [20]. The latter manifests itself as stress relaxation, creep and the rate-dependent mechanical response. For this purpose, several unified constitutive laws have been proposed, e.g., Freed and Walker [21], McLean and Dyson [22] and Chaboche [16]. They employ a set of evolution rules for kinematic and isotropic hardening in addition to the viscoplastic yielding rule. The widely used isotropic model of Chaboche is selected for further consideration, which is well-adopted for cyclic viscoplasticity in small strains.

The total strain $\boldsymbol{\varepsilon}$ is decomposed into the thermal $\boldsymbol{\varepsilon}^{\mathrm{th}}$, the elastic $\boldsymbol{\varepsilon}^{\mathrm{e}}$ and the viscoplastic $\boldsymbol{\varepsilon}^{\mathrm{vp}}$ strain components

$$\boldsymbol{\varepsilon} = \boldsymbol{\varepsilon}^{\mathrm{e}} + \boldsymbol{\varepsilon}^{\mathrm{vp}} + \boldsymbol{\varepsilon}^{\mathrm{th}}. \tag{1}$$

The viscoplastic strain rate is specified by the flow rule

$$\dot{\boldsymbol{\varepsilon}}^{\mathrm{vp}} = \dot{p}\boldsymbol{n}, \tag{2}$$

where $\dot{p}$ is the viscoplastic multiplier

$$\dot{p} = \left\langle \frac{J_2(\boldsymbol{s}-\boldsymbol{\chi}) - r}{K} \right\rangle^n \tag{3}$$

and $\boldsymbol{n}$ is the flow direction

$$\boldsymbol{n} = \frac{3}{2}\frac{\boldsymbol{s}-\boldsymbol{\chi}}{J_2(\boldsymbol{s}-\boldsymbol{\chi})}, \tag{4}$$

where $\boldsymbol{s}$ is the deviatoric stress tensor and $\boldsymbol{\chi}$ is the back stress tensor, which primary results from the internal stresses (in superalloys these are due to the γ/γ' interfaces). The power law function with the McCauley brackets in (3) is known as the Norton's law. The variable r defines the size of the elastic domain, K and n are the material parameters and J_2 means the equivalent stress function in the sense of von Mises. The isotropic hardening, that is the increase in the size of the elastic domain, is thus introduced through a functional dependence of the variable r on the accumulated viscoplastic strain p. The following relation is postulated

$$r = r_0 + Q\,(1 - \exp(-bp)) \tag{5}$$

with further material parameters Q denoting the saturated increase of r (a negative value of Q models the softening response) and b governing the hardening rate.

The back stress $\boldsymbol{\chi}$ follows an Armstrong-Frederick nonlinear kinematic hardening rule [23]

$$\dot{\boldsymbol{\chi}} = \frac{2}{3}C\dot{\boldsymbol{\varepsilon}}^{\mathrm{vp}} - d\boldsymbol{\chi}\dot{p}. \tag{6}$$

It evolves according to the direct hardening, which is collinear with the viscoplastic strain rate, and the dynamic recovery term, which is collinear with $\boldsymbol{\chi}$. The back stress may be thus seen as a competition between work hardening and recovery (dislocation climb and annihilation). The respective proportional coefficients C and d are the material parameters. Note that more complicated formulations

that consider both dynamic and static recovery terms may need to be used to express the temporal back stress relaxation

$$\dot{\chi} = \frac{2}{3} C \dot{\varepsilon}^{\mathrm{vp}} - d \chi \dot{p} - \left(\frac{J_2(\chi)}{M} \right)^m \frac{\chi}{J_2(\chi)}. \tag{7}$$

The last term governs the relaxation response and the predicted secondary creep rate, while having an almost insignificant impact on the prediction of a single hysteresis.

2.2. Incremental Lifetime Rules

It is generally recognized that the fatigue damage in metals is governed by irreversible inelastic flow, that is when the dislocation slip introduced during forward loading is not completely recovered during the reversed yielding. The damage variable $0 \leq D \leq 1$ is therefore, assumed to be driven by the yielding, more precisely the damage rate $\dot{D}$ is postulated to be a function of the flow rate $\dot{p}$. The lifetime rule is thus expressed as another evolution equation, considering D as an additional history variable. Such an incremental formulation couples naturally the constitutive model for deformation and the lifetime rule, emphasizing their dependence on the loading path. It is further assumed in this subsection that the damage variable does not significantly influence the macroscopic response so that the lifetime computation is performed in the post-processing analysis. Although the stabilized response might be macroscopically observed after N_{s} cycles, the fatigue damage is assumed to occur on the microscopic scale due to interaction of defects and dislocations. The lifetime is then calculated from the contribution of the single saturated cycle to damage ΔD_{s}

$$N_{\mathrm{f}} = N_{\mathrm{s}} + \frac{1 - D(N_{\mathrm{s}})}{\Delta D_{\mathrm{s}}} \approx \frac{1}{\Delta D_{\mathrm{s}}}. \tag{8}$$

A linear relation between $\dot{D}$ and $\dot{p}$ is proposed in [12,24]

$$\dot{D} = \left(\frac{Y}{A} \right)^m \dot{p}, \quad p > p_D. \tag{9}$$

Damage does not initiate below a threshold for the accumulated plastic strain p_D. The intensity of the damage rate is determined by the energy density release rate Y and so indirectly by the stress; m and A are two material parameters. The model was successfully applied for LCF tests. An extension to high-cycle fatigue (HCF), where damage happens microscopically even if the macroscopic load remains below the yield or failure stress, is derived in a two-scale CDM model [12]. The microscopic local stresses may be higher because of structural inhomogeneity. This scale phenomena was captured for case of spherical inclusions embedded into the matrix. Fatigue is promoted by dissipation on the microscale, where the model uses an asymptotic fatigue limit as a parameter. The two-scale model realistically predicts fatigue response, however it requires determining additional material parameters related to the extension on the microscale.

A similar empirical rule is presented in [25], which uses a nonlinear dependence on $\dot{p}$

$$\dot{D} = \left(\frac{J_2(\boldsymbol{s})}{A} \right)^m \left(\frac{\dot{p}}{\dot{p}_0} \right)^n \dot{p}_0 \tag{10}$$

with a temperature-independent scaling parameter $\dot{p}_0$. The exponent n describes the rate-dependence of the lifetime rule. It reduces to zero for a pure time-dependent behavior and achieves unity in the rate-independent limit. The parameters $\dot{p}_0$ and n are sensitive to the hold-times within the LCF tests, unlike the parameters A and m which are obtained from the conventional LCF tests. The lifetime evaluations of the hot work steels [26] were efficiently carried out by taking $N_{\mathrm{s}} = 3$. Note that the effect of creep is pronounced in the lifetime model (10) through the introduction of stress. This idea

was earlier suggested in the works of Krempl [27,28] who basically replaced the plastic strains in the lifetime models of Majumdar [29,30]

$$\dot{D} = C_0 \left|\varepsilon^{\mathrm{P}}\right|^m \left|\dot{\varepsilon}^{\mathrm{P}}\right|^n, \tag{11}$$

by stresses, where ε^{P} and $\dot{\varepsilon}^{\mathrm{P}}$ are the plastic strain and strain rates in the uniaxial case. Under multiaxial fatigue they read as the respective values for current plastic shear strain and strain-rate on the plane of the maximum plastic shear strain range. This is reasonable for those situations when the crack initiation and early propagation occur in the shear plane [31].

Another approach for modeling the lifetimes of the LCF tests relies on the time to creep rupture $t_{\mathrm{f}}(\sigma, T)$. The damage rate for creep under assumption of linear damage rule gets a simple form [32]

$$\dot{D} = \frac{1}{t_{\mathrm{f}}(\sigma, T)}, \tag{12}$$

where the rupture time for continuously changing stresses and/or temperatures is required. This method yields reasonable predictions for some Ni-base superalloys [33], provided the life time under LCF and under creep conditions must be controlled by the same dominant damage mechanism. It was indeed observed in this particular investigation, where the oxidation assisted crack growth at grain boundaries mainly resulted in the both creep and fatigue failures. Danzer has introduced the parameter r in order to quantify the difference between the creep and fatigue damage conditions [33]

$$r = \frac{\dot{p}}{\dot{\varepsilon}_{\mathrm{s}}(\sigma, T)}. \tag{13}$$

It compares the inelastic strain-rate in the cycle with the steady state rate $\dot{\varepsilon}_{\mathrm{s}}(\sigma, T)$ in a creep test at the same stress and temperature. The ideal applicability of (12) requires the r values close to unity, whereas the restriction $1 \leq r \leq 10$ has been shown to be practically acceptable. The model significantly overestimates the fatigue lifetime once the strain rates in the fatigue tests are much higher than in creep i.e., $r \gg 1$. Franklin [34] has suggested a slightly modified equation

$$\dot{D} = \frac{1}{t_{\mathrm{f}}(\sigma, T)} \left(\frac{\dot{p}}{\dot{\varepsilon}_{\mathrm{s}}(\sigma, T)}\right)^n, \tag{14}$$

where the positive parameter n reflects the increased damage response of the material under creep and fatigue as compared to that in a steady state creep. The obtained rule is formally similar to the lifetime rules (9) and (10), which are also driven by the yield rate but refer to the stress state unlike the model (14), which is related to the rupture time under creep. A comparative study of (12) and (14) in case of a cast Co-base superalloy is presented in [35]. Both models show reasonable correlation with results of the LCF tests, except for the tests at higher strain rates when the creep dominant model (12) is no longer applicable. The authors also reported less accurate prediction of the TMF tests which lifetimes were systematically overestimated by the both models. In order to get a better prediction of TMF loadings, a creep phasing factor is defined [36]

$$\dot{D}_{\mathrm{cr}} = A \, \exp\left[-\frac{1}{2}\left(\frac{(\dot{\varepsilon}^{\mathrm{th}}/\dot{\varepsilon}^{\mathrm{m}}) - 1}{\xi_{\mathrm{cr}}}\right)^2\right] \dot{\varepsilon}_{\mathrm{s}}(\sigma, T) \tag{15}$$

which particularly enhances the damaging effect of creep under IP loading in contrast to the more harmless OP conditions. Here A is a scaling factor, ξ_{cr} denotes the creep phase parameter which takes values between 0 and 0.5, $\dot{\varepsilon}^{\mathrm{th}}/\dot{\varepsilon}^{\mathrm{m}}$ is the ratio of thermal to mechanical strain rates under the uniaxial consideration.

Some approaches [37,38] divide the fatigue-creep damage into a cyclically induced damage D_{fat} and a time-dependent creep one D_{cr} in order to emphasize that these mechanisms are related to time differently. Thus, the damage rates by Krempl are calculated in the same manner (10) for creep and fatigue terms while differ only in the used material parameters. Both rates $\dot{D}_{\mathrm{cr}}$ and $\dot{D}_{\mathrm{fat}}$ contribute linearly to the total damage

$$\dot{D} = \dot{D}_{\mathrm{fat}} + \dot{D}_{\mathrm{cr}}. \tag{16}$$

Equation (8) can be then rewritten as

$$\frac{1}{N_{\mathrm{f}}} = \frac{1}{N_{\mathrm{fat}}} + \frac{1}{N_{\mathrm{cr}}}, \tag{17}$$

where N_{fat} and N_{cr} are related with the respective fatigue ΔD_{fat} and creep ΔD_{cr} damages associated with a saturated loading cycle (8). Majumdar proposes a lifetime model which does not link to the linearity assumption (16)

$$N_{\mathrm{f}} = N_{\mathrm{cr}} \left(\sqrt{1 + 2\frac{N_{\mathrm{fat}}}{N_{\mathrm{cr}}}} - 1 \right). \tag{18}$$

Note that both Equations (17) and (18) reproduce the pure fatigue lifetime N_{fat} if the cyclically induced damage $\dot{D}_{\mathrm{fat}} \gg \dot{D}_{\mathrm{cr}}$ is dominant.

2.3. Application to an Austenitic Cast Iron under TMF

The life assessment of a cast iron EN-GJSA-XNiSiCr 35-5-2, also known as Ni-Resist D-5S, is demonstrated in this subsection. The alloy was chosen since it is often used in exhaust turbochargers, which are subjected to severe TMF conditions. The comprehensive experimental program consisted of LCF, TMF, creep and complex strain-controlled cyclic tests (complex LCF).

2.3.1. Experimental Procedure

The alloy was cast in form of Y II samples. All tests were carried out on round specimens with the diameter of 6 mm.

The specimens with shoulder a head and a measuring length of 16 mm were used for the LCF and complex LCF tests. These were carried out on a 100 kN universal testing machine, type INSTRON, in conjunction with an electrical MTS extensometer with a measuring length of 14.1 mm. Two thermocouples of type S were used for the temperature measurements. The specimens were heated up with a resistance furnace and then held for one hour at the test temperature before starting the tests in order to achieve a uniform heating. To investigate the influence of hold times, the specimens were loaded in tension for 180 s in each cycle. The LCF tests were carried out in strain control at $R = -1$, with a strain rate of 10^{-3} s^{-1} and at temperatures of 20 °C, 300 °C, 500 °C, 600 °C, 700 °C, 800 °C and 900 °C. The complex LCF tests included three series of cycles separated by hold times of one hour (stress relaxation). The cycles within each series had the same strain amplitude, which increased from 0.2% for the first series to 0.9% for the last one, while the loading ratio $R = -1$ was kept unchanged. Moreover, the hystereses were driven at various strain rates 10^{-5} s^{-1}, 10^{-3} s^{-1} and 10^{-2} s^{-1} in order to capture the rate-dependency of the mechanic response.

The specimens with a shaft head and a measuring length of 16 mm were used for the TMF tests. These were carried out on air on a MTS servo-hydraulic testing machine in conjunction with an electrical MTS extensometer with a measuring length of 10 mm. The specimens were heated inductively, cooled by free convection in air and by heat runoff into the water-cooled specimen grips. To monitor the temperature, a type S thermocouple was welded on in the middle of the measuring length. This form of attachment could be chosen because no failure was caused by the welding spot. The TMF tests were performed by controlling the total elongation with a mechanical strain ratio $R = -1$ and a temperature rate of 5 K/s. The TMF tests were carried out in the temperature intervals

with the same lowest temperature 400 °C and various high temperatures 700 °C, 800 °C and 900 °C, as summarized in Figure 1c. The 180 s hold times at the highest temperature reproduce the service conditions of the component. The 5% load drop in tension was defined as the failure criterion for LCF and TMF tests.

The specimens with a thread head and a measuring length of 50 mm were used for the creep tests. The system was equipped with a radiation furnace (3 zones). The strain was measured by an extensometer of type HBM with a measuring length of 20 mm. The creep tests were performed at 700 °C, 800 °C and 900 °C. The temperature was measured with three thermocouples of type S, which were tied within the measuring length.

2.3.2. Results and Analysis

The lifetime model uses a slightly modified incremental rule (10). In particular, the total back stress instead of the equivalent stress controls the accumulation rate of the damage variable according to

$$\dot{D} = \left(\frac{J_2(\chi)}{A}\right)^m \left(\frac{\dot{p}}{\dot{p}_0}\right)^n \dot{p}_0. \tag{19}$$

Moreover, another independent back stress variable was added to the deformation model of Chaboche in order to provide a more accurate description of the viscoplastic yielding [25,26].

All material parameters are temperature-dependent and have been determined from uniaxial isothermal complex LCF and creep tests. The rate-dependency is reproduced by parameters K and n in (3). The isotropic (5) and kinematic hardening (7) influence the cyclic response, whereas the static recovery term in (7) is calibrated separately with the creep tests and stress relaxation during the hold times. The calibrated deformation model has been verified on the basis of the non-isothermal cyclic tests. For this purpose, the results of direct numerical simulations were compared with the experimental observations on in phase (IP) and 180° out of phase (OP) fatigue tests. The hystereses at the half lifetime are in good agreement, as demonstrated in Figure 1.

The incremental lifetime rule (19) was adjusted to the LCF tests. Almost all tests correlate with the lifetime model predictions within the usual factor 2 scatter band.

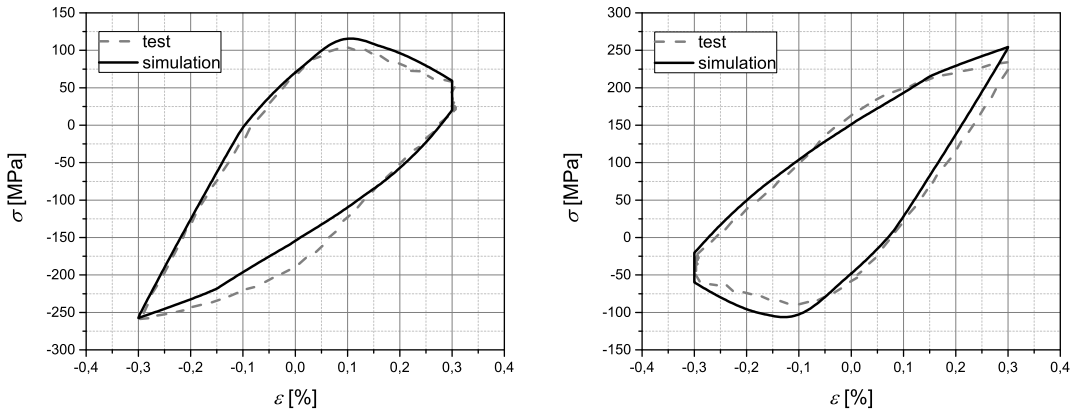

(**a**) (**b**)

Figure 1. *Cont.*

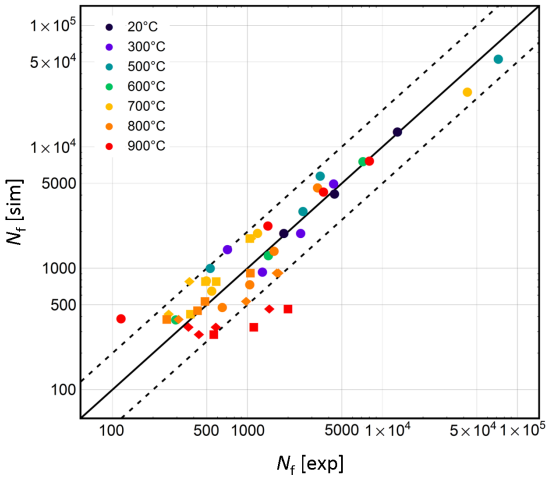

(**c**)

Figure 1. Calibration of the lifetime model for the Ni-Resist D-5S alloy. The deformation response of TMF tests in the temperature range 400 °C to 900 °C is depicted under (**a**) IP and (**b**) OP conditions. (**c**) Calculated versus experimentally determined number of cycles to failure for LCF and TMF tests at various conditions. The life assessment plot uses the incremental lifetime rule (19). The filled circles (●) represent LCF tests, the squares (■) represent non-isothermal IP tests and the diamonds (◆) show non-isothermal OP tests. The highest temperature of the TMF tests is indicated by the color.

2.4. Extension of the Incremental Lifetime Rules to Single Crystals

The evaluation of deformation fields and lifetimes in a single crystal should account for a distinct dependence on the crystallographic orientation (anisotropy). As a result, an appropriate deformation model for single-crystal superalloys requires an extension to the crystallographic slip systems, i.e., slip plane and slip direction. The widely used crystallographic model of Cailletaud [17] can be regarded as a one-dimensional form of the standard viscoplastic Chaboche model on each slip system. This model introduces the slip systems of the austenitic fcc lattice of the γ-matrix [39]. The viscoplastic strain rate $\dot{\boldsymbol{\varepsilon}}^{\mathrm{vp}}$ is given as the sum over shear strain rates $\dot{\gamma}_g$ on 12 octahedral and 6 cubic slip systems

$$\dot{\boldsymbol{\varepsilon}}^{\mathrm{vp}} = \sum_{g \in G_{\mathrm{oct}}} \dot{\gamma}_g \boldsymbol{\mu}_g + \sum_{g \in G_{\mathrm{cub}}} \dot{\gamma}_g \boldsymbol{\mu}_g, \tag{20}$$

where $\boldsymbol{\mu}_g$ denotes the orientation tensor corresponding to the slip system g. The viscoplastic shear strain rate is expressed similar to (3) as a power law function of the overstress in the slip system

$$\dot{\gamma}_g = \left\langle \frac{|\tau_g - \chi_g| - r_g}{K} \right\rangle^n \mathrm{sgn}(|\tau_g - \chi_g| - r_g). \tag{21}$$

The value of each parameter of the crystallographic model is associated with the respective family of the slip systems. For instance, K takes the value K_{oct} for the octahedral slip systems $g \in G_{\mathrm{oct}} = [1, 12]$, and is equal to K_{cub} for the cubic slip systems $g \in G_{\mathrm{cub}} = [13, 18]$. All other values, e.g., the resolved shear stress $\tau_g = \boldsymbol{\sigma} : \boldsymbol{\mu}_g$, the back stress χ_g and the isotropic hardening contribution r_g are specific for each slip system. Their scalar evolution equations keep the principal form of (5)–(7) by taking $\dot{\gamma}_g$ and $|\dot{\gamma}_g|$ instead of $\dot{\boldsymbol{\varepsilon}}^{\mathrm{vp}}$ and $\dot{p}$ respectively.

In the next step, an incremental lifetime rule for the anisotropic material should be proposed, which is consistent with the crystallographic structure. A straightforward usage of the isotropic incremental lifetime rules (9)–(14) to the single crystal superalloys is rather questionable. According to many investigations on small fatigue cracks [40–42], the Ni-base single crystals may exhibit crack propagation on the octahedral slip planes with the fracture surface manifesting a cleavage-like

appearance. This tendency is stronger at low or moderate temperatures and higher frequencies, while cracks usually propagate normal to loading direction independent of crystal orientation at high temperature [42,43]. This is opposite to the observations in polycrystalline materials, which macroscopic cyclic crack growth is dominated by the normal tensile load in the whole temperature and frequency ranges. It has been therefore, suggested that microcrack initiation during fatigue is caused by localized cyclic plastic deformation and shear decohesion on the octahedral slip planes [44]. The subsequent formation and propagation of the macroscopic cracks occur consequently along well-defined crystallographic planes. The propagation rate was found to correlate with the resolved shear stresses [41,45] and the plastic zone size [46] on the dominant slip planes. In view of this observations, a more promising approach in regard to formulating the incremental lifetime rule is thus to consider the cumulative fatigue damage induced by dislocation slip on each slip plane. In this way, the lifetime rule of Krempl (10) was adapted [47] to the crystal plasticity framework. Thereby, the resolved shear stress was included instead of the equivalent stress used for polycrystalline alloys

$$\dot{D} = \sum_{g \in G_{\mathrm{oct}}} \left(\frac{|\tau_g|}{s_{\mathrm{oct}}} \right)^{m_{\mathrm{oct}}} \left(\frac{|\dot{\gamma}_g|}{\dot{\gamma}_{\mathrm{oct}}} \right)^{n_{\mathrm{oct}}} \dot{\gamma}_{\mathrm{oct}} + \sum_{g \in G_{\mathrm{cub}}} \left(\frac{|\tau_g|}{s_{\mathrm{cub}}} \right)^{m_{\mathrm{cub}}} \left(\frac{|\dot{\gamma}_g|}{\dot{\gamma}_{\mathrm{cub}}} \right)^{n_{\mathrm{cub}}} \dot{\gamma}_{\mathrm{cub}}. \tag{22}$$

The life assessment by means of this incremental rule satisfactory fit the result of mechanical tests on the CMSX4 superalloy. The lifiteme rule was further modified in [38] due to split of the cyclic and time contributions to damage (26). This is because different mechanisms are assumed to be attributed to cyclic and creep damages. Namely rafting, formation of voids and initiation of microcracks from the voids and pre-existing micropores lead to degradation under creep, while the cyclic damage is related to the irreversible motion of dislocations during slip. As a consequence, the tests with various durations of a hold time within the loading cycle could be consistently reproduced, although the creep differently affected the material response.

A similar approach is proposed in [48], who correlated the viscoplastic work rate in all slip systems $\dot{W}^{\mathrm{vp}}$

$$\dot{W}^{\mathrm{vp}} = \sum_{g \in G_{\mathrm{oct}}} |\tau_g - \chi_g| \dot{\gamma}_g + \sum_{g \in G_{\mathrm{cub}}} |\tau_g - \chi_g| \dot{\gamma}_g. \tag{23}$$

with the rate of material deterioration. It is supposed that this measure of damage accounts for the combined impact of creep and fatigue. The reduction of lifetime at lower service temperatures is assumed to be attributed to fatigue in the macroscopically elastic regime. In other words, the failures due to elastic and inelastic fractures are treated as independent damage processes. Equation (17) is used with regard to each mechanism N^{e} and N^{vp} respectively

$$N^{\mathrm{e}} \propto \frac{1}{\sigma_{\mathrm{max}}^{m}}, \tag{24}$$

$$N^{\mathrm{vp}} \propto \frac{1}{\Delta {W^{\mathrm{vp}}}^{n}}, \tag{25}$$

where σ_{max} is the maximum principal stress and ΔW^{vp} is the viscoplastic work per the stabilized loading cycle. The life prediction criterion was successfully validated with the LCF and TMF tests on the single-crystal PWA1484 superalloy.

On the contrary, Tinga suggested a direct combination of a discrete fatigue damage and a continuous damage caused by creep. The accumulated fatigue damage is proportional to the number of cycles [38] and increases on ΔD_{fat} at each load reversal when forward slip is followed by backward slip. The creep part keeps the conventional time-incremental framework. The incremental form of (16) during a time increment δt is therefore, given as the summation of the contributions attributed to creep and fatigue

$$\delta D = \dot{D}_{\mathrm{cr}}\, \delta t + \Delta D_{\mathrm{fat}}, \tag{26}$$

where both D_{cr} and ΔD_{fat} follow the equations which are formally similar to (22) with the difference that the fatigue part uses the maximal values for the resolved shear stress and slip rate during the cycle, in contrast to the creep term which commonly takes the current values. This approach was applied to single crystal Ni-base superalloys in order to get a consistent prediction of slow and fast LCF tests.

3. Parametric Lifetime Models Based on the Fracture Mechanics Concepts

The parametric lifetime assessment relies on certain characteristics of hystereses as the inputs for an empirical lifetime rule, while the link to the deformation and loading history is not mandatory. The deterioration mechanisms are treated explicitly, which in combination with the life fraction rule, e.g., the linear life fraction summation (17), compute the lifetime reduction referring the appropriate damage. For instance, some materials experience enhanced deterioration because of oxidation related processes. Their impact on damage acceleration is then introduced as

$$\frac{1}{N_f} = \frac{1}{N_{fat}} + \frac{1}{N_{cr}} + \frac{1}{N_{ox}}. \tag{27}$$

Specific forms of the enviromental term are given in [49] for the impact on the lifetime till crack initiation and for the influence on the crack growth rate [50,51]. They are based on a parabolic rate law of the oxide layer. The further focus is placed on the first two terms attributed to the mechanical origins of damage.

A large class of the parametric models are the energy-based lifetime models [7,8,10] mentioned in the introduction. They correlate fatigue lives with a hysteresis energy density, since this includes both stress and strain information. The plastic strain energy density (surface of hysteresis loop [8]) computed for the fatigue tests on the Ni-Resist D-5S alloy is plotted in Figure 2. The values of the plastic work are significantly scattered, in particular the TMF tests result in systematically lower values than those obtained for the LCF tests. The plastic strain energy density is therefore, not a suitable damage parameter for estimation of lifetimes of the Ni-Resist D-5S alloy.

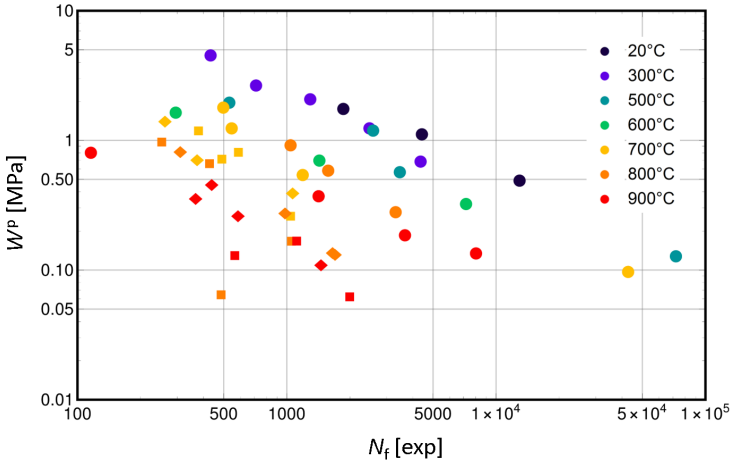

Figure 2. Plastic strain energy density computed as the area inside the closed cyclic loop at the half lifetime (see Figure 1a,b) versus number of cycles to failure. The filled circles (●) represent LCF tests, the squares (■) represent non-isothermal IP tests and the diamonds (◆) show non-isothermal OP tests. The highest temperature of the TMF tests is indicated by the color.

Among the class of parametric models, the approaches addressing the fracture mechanical concepts are of particular interest. This is because of their efficiency for those situations when the component lifetime is dominated by the propagation of the microcracks and not their incubation stage. Such lifetime models and their application to the Ni-Resist D-5S alloy are discussed in what follows.

3.1. Fatigue Lifetimes by Microcracks Growth

According to Neumann [52], the fatigue crack growth in a notched specimen is caused by irreversible repeating sequence of sharpening and blunting of the crack tip. This occurs due to alternating slip on two slip systems which intersect on the crack front. The crack advances on an increment da that is on the order of the cyclic crack-tip opening displacement $\Delta\delta_t$, provided that the latter exceeds a critical value

$$\frac{da}{dN} = \beta \Delta \delta_t^B. \tag{28}$$

This approach is thus based on the idea that the crack opening displacement δ_t is a measure of plastic strain at the crack tip and controls the crack propagation per cycle. A simple relation between δ_t and the fracture parameter contour J-integral is given for the fundamental model of Dugdale for a mode-I crack in an elastic/perfectly plastic material [53]

$$\delta_t = \frac{J}{\sigma_Y}, \tag{29}$$

and extended [54] for power law hardening materials with the Ramberg Osgood hardening exponent n' as

$$\delta_t = d_{n'} \frac{J}{\sigma_Y}, \tag{30}$$

where $d_{n'}$ is a known constant dependent on n', σ_Y is the yield stress. Note that this equation holds also for the cyclic $\Delta\delta_t$ crack-tip opening displacement, just replacing the J-integral in (30) with the cyclic ΔJ-integral, and introducing cyclic yield stress σ_{cY} instead of the monotone one σ_Y

$$\Delta\delta_t = d_{n'} \frac{\Delta J}{\sigma_{cY}} = d_{n'} \frac{Z_D}{\sigma_{cY}} a, \tag{31}$$

since $\Delta\delta_t$ should be proportional to a for dimension consistency, the parameter Z_D is introduced such that aZ_D is an approximation of ΔJ-integral.

In the present consideration the issue is however on transferring the fracture mechanics concepts to initially smooth specimens. It is believed that the cyclic crack-tip opening displacement $\Delta\delta_t$ is a suitable loading parameter on the microcrack size scale, and correlates with the lifetime. The physical interpretation of using the fracture mechanical parameters on this finer scale goes beyond the current scope, including the questions whether the size of the process zone is negligibly small compared to the dimensions of the microcracks, an increased impact of microstructure on the crack path at the scale of microcracks and neglecting non-singular terms in the asymptotic approximation [53].

The model proposed by Riedel [55] introduces thus the damage parameter D_{fat} which quantifies the damaging effect of one loading cycle due to microcracks growth. Its relation to $\Delta\delta_t$ and the current crack depth a is given as

$$\Delta\delta_t = d_{n'} D_{fat}\, a. \tag{32}$$

Integrating (28) with (32) between an initial size a_0 of the order of magnitude of a few μm and the final size a_f of the order of magnitude of a few mm yields relationship of the type (8)

$$N_{fat} = \frac{A}{D_{fat}^B}, \tag{33}$$

where a_0, a_f and β from (28) are condensed in the parameter A, which together with B are adjustable parameters. The link of the damage parameter to the contour integral can be established due to a direct comparison of (32) with (31), what leads to the expression

$$D_{fat} = \frac{Z_D}{\sigma_{cY}}. \tag{34}$$

Note that cyclic yield stress decreases at high temperatures. On the one hand this leads to an increased uncertainty in determination of σ_{cY} and so of D_{fat}. On the other hand, the scatter of the damage parameter (34) reduces with respect to the temperature of the tests. In this context, using parameter D_{fat} is more advantageous than applying the energy measure W^P shown in Figure 2.

For small semi-circular surface cracks in infinite half-space, according to Heitmann [56], the time-independent solution for Z_D consists of contributions of elastic w^e and plastic w^p strain energy densities with the coefficients

$$Z_D = 2.9\, w^e + 2.4\, w^p, \tag{35}$$

$$w^p = \frac{\Delta\sigma\Delta\varepsilon^p}{\sqrt{1+3n'}}. \tag{36}$$

Here $\Delta\sigma$ and $\Delta\varepsilon^p$ are the ranges of stress and plastic strain per cycle. The crack closure effect is introduced by taking in the elastic strain energy density the effective stress range $\Delta\sigma_{eff}$ above the crack opening stress σ_{op}

$$\Delta\sigma_{eff} = \sigma_{max} - \sigma_{op}, \tag{37}$$

$$w^e = \frac{\Delta\sigma_{eff}^2}{2E}. \tag{38}$$

Vormwald and Seeger proposed later another approximation for the cyclic ΔJ-integral which relies on the effective values in the plastic term [57]

$$Z_D = 2.48\, w^e + 1.02\, w^p, \tag{39}$$

$$w^p = \frac{\Delta\sigma_{eff}\Delta\varepsilon_{eff}^p}{\sqrt{n'}}, \tag{40}$$

where the effective plastic strain range is defined based on (37) as $\Delta\varepsilon_{eff}^p = \varepsilon_{max} - \varepsilon_{op} - \Delta\sigma_{eff}/E$. The relations (35)–(36) and (39)–(40) are very similar: they both include elastic and plastic contributions with different coefficients, which however insignificantly affect the computation of the lifetime. The principal qualitative distinction is that the latter accounts for the crack closing effect on the plastic term.

The effective stress range cannot be evaluated directly from a hysteresis. It is therefore, useful to establish a link between it and the hysteresis stress range in relation with the loading ratio $R = \frac{\sigma_{min}}{\sigma_{max}}$

$$\Delta\sigma_{eff} = U(R)\,\Delta\sigma. \tag{41}$$

Various empirical expressions have been used in the literature for the function $U(R)$, for instance that one by Heitmann [56]

$$U(R) = 3.72(3-R)^{-1.74}, \tag{42}$$

by Schijve [58]

$$U(R) = 0.55 + 0.33R + 0.12R^2, \tag{43}$$

or by Newman [59], who used a third order polynomial function which coefficients depended on $\frac{\sigma_{max}}{\sigma_Y}$. It should be noted that the plasticity-induced crack closure differently affects the physically short and long cracks. The crack closure gradually develops during the crack growth until achieves a saturated inhibiting impact on the propagation rate. This leads to the physically short crack effect, which emphasizes that short cracks can propagate below the crack threshold stress intensity and grow faster than long cracks. Thus using (41) with function $U(R)$, which depends only on the loading ratio and reflects the state once the crack-closure is fully developed, may be a significant simplification for

those situations when the microcrack growth is regarded as the essential deterioration mechanism. The reader is referred to [60] for a deeper insight into the fatigue crack closure phenomena.

3.2. The Impact of Creep Deformation on Damage Due to Microcrack Growth

The incorporation of creep into the parametric lifetime models can be related with damage or deformation processes. In the first case, the creep damage is considered as another mechanism of failure, for example creep damage by void or microcrack coalescence, in addition to the rate-independent fatigue. The respective lifetime N_{cr} in (27) is then computed by applying (12)–(15) to the stabilized hysteresis. An example of this approach is demonstrated in [61], who used an integral form of the creep damage accumulation after Danzer and Franklin (14). In the second case, creep deformation influences the asymptotic field and increases the crack tip opening displacement $\Delta\delta_t$ due to time-dependent blunting of the microcrack tip. The description of both creep deformation and fatigue damage are then combined in the same fracture mechanical framework. For the sake of consistency, the attention is further focused on the latter situation.

As in the case with ΔJ-integral, the C^*-integral is path-independent and applicable as a crack tip loading parameter under steady state creep [53]. According to Riedel [62], it is proportional to

$$C^* \propto 2.4\,\frac{\sigma\dot{\varepsilon}^{cr}}{\sqrt{1+3/n}}. \tag{44}$$

where σ is the peak stress, $\dot{\varepsilon}^{cr}$ is the creep rate and n is the Norton exponent. Note the similarities between (36) and (44). Parameter (44) was taken in the integral form over the tensile portion of the loading history in order to compute the creep damage value, assuming that the compressive hold period did not contribute to creep damage [63]. The model yielded reasonable predictions for TMF lives of the cast nickel-base superalloy MAR-M247. When $n = 1/n'$, an HRR-type asymptotic field exists at the crack tip that results from plastic and stationary creep deformations. Consequently, the terms associated with Z_D and C^* can be combined to form the creep-fatigue damage parameter D_{TMF}, which can be calculated analogically to (34)

$$Z_{TMF} = 2.9\,\frac{\Delta\sigma_{eff}^2}{2E} + 2.4\,\frac{\Delta\sigma\left(\Delta\varepsilon^p + \Delta\varepsilon^{cr}\right)}{\sqrt{1+3n'}}\left(1+\frac{\Delta\varepsilon^{cr}}{\Delta\varepsilon^p}\right)^{n'}. \tag{45}$$

It assumes separation into plastic and creep strains and requires thus an appropriate test program to determine the creep contribution. This damage parameter is used [64,65] to fit the model parameters in (33) and to evaluate the mechanical portion in the total lifetime (27), that is $N_{fat}^{-1} + N_{cr}^{-1}$ is replaced by N_{TMF}^{-1}

$$N_{TMF} = \frac{A}{D_{TMF}^B}, \tag{46}$$

$$D_{TMF} = \frac{Z_{TMF}}{\sigma_{cY}}. \tag{47}$$

As demonstrated in [64], it provides very satisfactory lifetime assessments of complex TMF tests on the austenitic stainless steel AISI304L, including the IP loadings which are much more detrimental since creep damage exclusively develops because of the combination of high temperatures and tensile stresses.

Another formulation for high temperature applications is proposed in [55,66], which in contrast to (45) does not distinguish between creep and instantaneous plasticity. The fatigue part of the formulation is driven by the damage parameter Z_D from (34). A correction factor $f(t, T, \sigma)$ is defined

in order to incorporate the influence of creep on the crack-tip opening displacement. Its temperature sensitive modification is denoted by Z_{TMF}

$$Z_{\mathrm{TMF}} = f(t, T, \sigma)\, Z_{\mathrm{D}}, \tag{48}$$

$$f(t, T, \sigma) = \left(1 + \alpha \exp\left[-\frac{Q_{\mathrm{cr}}}{RT_{\mathrm{ref}}}\right] \int_t \sigma_{\mathrm{cY}}^{n-2}(T)\, |\sigma(t) - \sigma_{\mathrm{min}}|\, \exp\left[-\frac{Q_{\mathrm{cr}}}{RT}\right] \mathrm{d}t\right)^{1/n}, \tag{49}$$

where $f(t, T, \sigma)$ is a thermally activated function of stress, normalized by the cyclic yield stress and integrated over the cycle time. This function describes the time-dependent contribution to $\Delta\delta_{\mathrm{t}}$ with increasing temperature T and loading duration. T_{ref} is a reference temperature taken here to 500 °C, n is the Norton exponent, Q_{cr} is the activation energy for creep and α is an adjustable parameter. The Z_{TMF} parameter reduces to Z_{D} at ambient temperatures where creep effects are negligible. In what follows, the parametric model based on (48) is calibrated for Ni-Resist D-5S for comparison with the incremental lifetime rule (19).

3.3. Application to the Austenitic Cast Iron under TMF

As case studies, both the instantaneous formulation from Section 3.1 and the time-dependent one from Section 3.2 were investigated. They included Equations (35)–(38) with the definition (42) of $U(R)$. In addition, the time-dependent formulation used the thermally activated damage accordingly to (48) and (49). For uniaxial loadings, the quantities required in (35) and, consequently for computation of the respective damage parameters D_{fat} in (34) and D_{TMF} in (47), can be gained solely from the stabilized hysteresis loop. These were taken from the same hystereses at the half lifetime, as shown in Figure 3. The parameters A and B in (46) and α, Q_{cr} and n appearing in (49) were determined by a non-linear regression procedure on the valid isothermal and non-isothermal test data at the whole temperature range, as provided in Section 2.3 for the Ni-Resist D-5S alloy. The results obtained for the damage parameters are depicted in Figure 3a,b. The values of D_{fat} are noticeably underestimated for the TMF tests, which comprise hold times. Their contribution to creep and thus to the damage parameter D_{TMF} is properly captured by the time-dependent model, demonstrating a better correlation with the experimental observations. The respective lifetime plot (46) is shown in Figure 3c.

It is worth noting that a two step regression procedure can be carried out, which separately determines the parameters A and B from the LCF at low and moderate temperatures, whereas the factor α can be obtained by fitting the non-isothermal IP tests. Such a procedure is in line with the formulation (48) and (49) where Z_{D} controlling the low temperature fatigue and $f(t, T, \sigma)$ governing the additional crack opening displacement due to creep are multiplicatively combined. The two step procedure leads however to a too high value of α and consequently to a quite poorer conservative prediction for the high temperature tests.

As seen from the comparison between Figures 1c and 3c, the parametric model is less accurate than the incremental lifetime model. The latter has however overall more parameters because these are specified for each test temperature. In view of the complexity of the testing program, which comprises LCF and TMF loadings, and taking into account the simplicity of the parametric model attributed to the microcrack growth, the agreement must be considered as satisfactory. It was suggested that the alloy has high oxidation strength and the oxidation-induced embrittlement was not considered to enhance the fatigue crack growth. An intergranular creep damage with wedge-type cracks was indicated by metallographic investigations under these testing conditions [67].

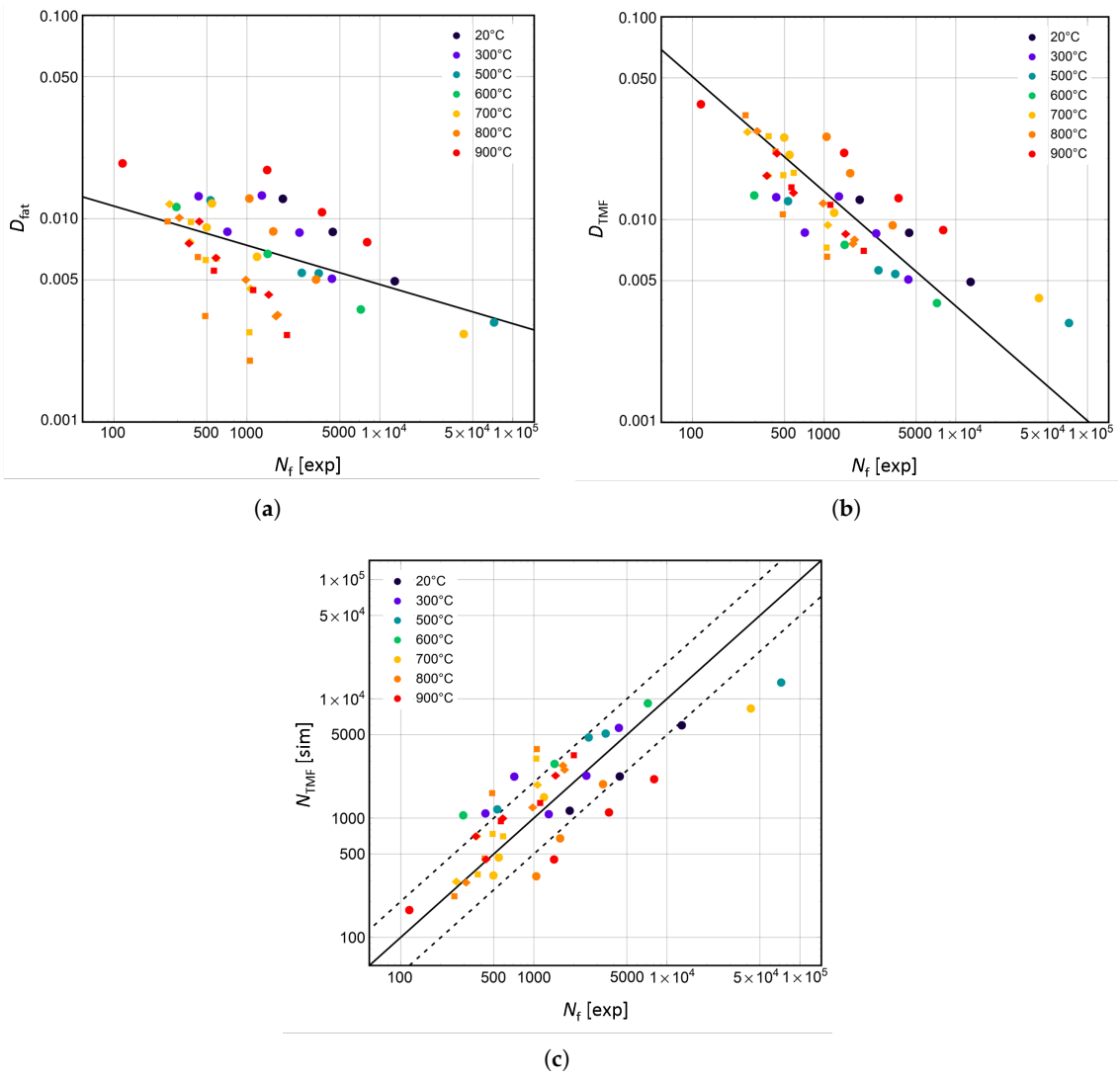

Figure 3. Predictions of the microcracks growth lifetime models for the Ni-Resist D-5S alloy. (**a**) Instantaneous damage parameter (34)–(36), (**b**) accounting for creep (47)–(49) and (**c**) the respective number of cycles to failure (46) for LCF and TMF tests at various conditions. The filled circles (●) represent LCF tests, the squares (■) represent non-isothermal IP tests and the diamonds (◆) show non-isothermal OP tests. The highest temperature of the TMF tests is indicated by the color whereas the lowest temperature of 400 °C was the same for all TMF tests.

4. Accelerated Cyclic Integration in Time

4.1. Review of Approaches

The approaches described in the previous sections are particularly convenient in engineering practice if a structure under cyclic loading reveals the asymptotic response. This can be determined for inelastic solids e.g., by the direct cycle analysis [68] implemented in the commercial program Abaqus or the residual stress decomposition method [69], which both adopt the Fourier transformation in time. Otherwise, if the stabilized response does not exists, the integration of the whole loading history is required in order to reflect a realistic degradation of the material in each loading cycle. A key challenge here is to address the issues related to fatigue on the structural level. This is due to the enormous computational costs arising from solving each load cycle by conventional temporal incremental integrations or employing the parametric methods. Despite the permanent increase of computational resources and algorithmic performance, a successful approach is rather based on

the development of multiscale in time integration schemes. In contrast to the previously discussed lifetime models, which *approximate the lifetime* as a function of the loading amplitude, crack-tip opening displacement, incrementally accumulated cyclic damage etc., the accelerated approaches *approximate the fatigue loading history* keeping the numerical efforts acceptably low. Thus the stress redistribution and permanent deformations are properly taken into account.

The accelerated integration methods rely on an underlying extrapolation of the history variables. Their growth per cycle are first evaluated by the incremental integration of the structural response. Afterwards, the damage state is estimated after a large number of the subsequent loading cycles by plugging the growth rates in the extrapolation scheme. The displacement and other response fields are obtained by finite element method (FEM) to fulfill the structure equilibrium under the extrapolated damage state. In this way, a remarkable speedup is achieved because the number of cycles to be fully integrated dramatically decreases. The described procedure is well known in the literature as the cycle jump method [15].

Further sophisticated methods consider fatigue as a two-scale phenomenon in time: the fine time scale (τ) is attributed to the oscillatory loadings while the coarse scale (Y) is related to the nonlinear structure response due to slow evolution of the history variables. The scale separation assumption implies that accumulation of damage is negligible on the fine scale. The history variables and the response fields can be then approximated using an asymptotic expansion about the macrochronological scale. As a consequence, the global equilibrium should be satisfied separately on the fine and coarse scales, which interact through the constitutive behavior. The capability of the method was demonstrated for a ceramic composite [70] simulating its material response by a continuum damage model. In line with the assumption of the scale separation, the equilibrium state over the fine temporal scale was taken to be unaffected by the change in the damage state [71]. The respective equilibrium problem becomes linear and can be efficiently solved with the conventional methods of the linear algebra. Application of the method to a viscoplastic cyclic deformation was shown on example of polymer materials [72]. A particular attention was paid to capturing the oscillations of the viscoplastic strains when the loading ratio R tends towards unity.

Another group of approaches are the transformation-based temporal integration methods. They take advantage of the temporal scale separation for approximation of the response fields by a series. Thus the Fourier transformation-based integration (FTTI) was represented in [73,74] which searches for the displacement field as a Fourier series with angular frequency ω

$$\boldsymbol{u}(\mathrm{Y},\tau) = \sum_{k\in\mathbb{Z}} \boldsymbol{u}_k(\mathrm{Y}) \exp(ik\omega\tau), \tag{50}$$

whose basis functions reproduce the oscillatory fine scale, whereas the Fourier coefficients $\boldsymbol{u}_k(\mathrm{Y})$ undergo the evolution on the coarse scale. This is correlated with the evolution of the history variables, including damage, by means of the adaptive cycle jump method of various orders. A further idea behind the FTTI method is that the Fourier coefficients can be in advance computed from linear equilibrium problems. Consequently, integration of a single load cycle is performed with the prescribed displacement field (50). This is much more efficient than the conventional single scale integration and results therefore, in an additional speedup of FTTI. The performance of another transformation-based approach WATMUS has been investigated in [75], where the wavelet functions were used to resolve the micromechanical response of a polycrystalline viscoplastic aggregate over the fine time scale. The applicability of the method was later demonstrated for accelerated integration of coupled electromagnetic and structural dynamics problems [76]. In what follows, the FTTI technique is demonstrated for a finite element simulation of a viscoplastic solid exhibiting damage which is governed by viscoplastic yielding.

4.2. Benchmark Example of the Viscoplastic Cyclic Response Treated by FTTI

A notched plate is considered under the isothermal condition and a compressive sinusoidal traction applied on the top boundary, see Figure 4a. For symmetry reasons, only one fourth of the specimen is analyzed using symmetric boundary conditions on the horizontal and vertical axes of symmetry. The analysis is performed under plane strain conditions. The FE model is meshed with quadrilateral elements.

The constitutive behavior assumes influence of damage on the deformation state. The Hooke's law relates thus the stress tensor σ with the elastic strain tensor by means of the damaged material stiffness

$$\boldsymbol{\sigma} = (1 - D)\boldsymbol{C} : (\boldsymbol{\varepsilon} - \boldsymbol{\varepsilon}^{\mathrm{vp}}). \tag{51}$$

Without loss of generality, the thermal strain is put to zero in (1) and therefore, is omitted in (51). The damage rate is driven by the equivalent viscoplastic strain rate $\dot{p}$ as

$$\dot{D} = (1 - D)\frac{\dot{p}}{\dot{p}_0}, \tag{52}$$

where $\dot{p}_0$ is a model parameter.

The reference FE simulation is obtained by a straightforward cycle-by-cycle integration over the fatigue loading history. It reveals a pronounced stress redistribution in the reduced section of the plate. Consequently, the initially most stressed place (marked as position 1 in Figure 4a) does not result in the failure, which location on the curved boundary is denoted by 2. The continuous increase of the damage variables in the both places is depicted in Figure 4b. The solutions obtained by the accelerated FTTI technique are represented on the same graph by the cycles. These correspond to the extrapolation jumps on the coarse time scale. A two step procedure is used for a higher extrapolation accuracy

$$D\left(\mathrm{Y} + \frac{\Delta \mathrm{Y}}{2}\right) = D(\mathrm{Y}) + \frac{N}{2}\Delta_c D(\mathrm{Y}), \tag{53}$$

$$D(\mathrm{Y} + \Delta \mathrm{Y}) = D(\mathrm{Y}) + N\,\Delta_c D\left(\mathrm{Y} + \frac{\Delta \mathrm{Y}}{2}\right), \tag{54}$$

where the extrapolation length comprises N loading cycles. $\Delta_c D(\mathrm{Y})$ and $\Delta_c D\left(\mathrm{Y} + \frac{\Delta \mathrm{Y}}{2}\right)$ are the cyclic increases of damage at the beginning and in the middle of the jump respectively. They have to be calculated once the global equilibrium is restored after each extrapolation step, that is after update of the Fourier approximation (50). A detailed description for FE solving with regard to the Fourier coefficients is provided in [73].

The obtained FTTI solution perfectly reproduce creep deterioration and stress redistribution while reducing the computational costs of the particular simulation by one order of magnitude. The varying length of the extrapolation jumps is due to an adaptive time stepping which controls the errors resulting from the extrapolation of the history variables. The discrepancy between the FTTI and reference solutions close to the onset of failure, as seen in Figure 4b, is attributed to an inherit error associated with loss of periodicity of the displacement field.

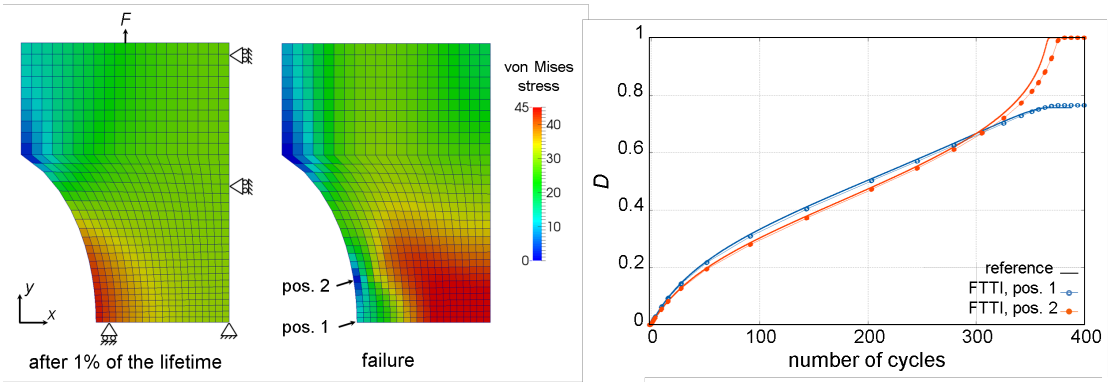

(**a**) (**b**)

Figure 4. (**a**) Evolution of the stress distribution map during the lifetime under sinusoidal load oscillations applied on the top boundary in *y*-direction. (**b**) Evolution of damage in the highly stressed regions of the domain.

5. Discussion and Conclusions

A review of some computational approaches for assessment of service lives of hot metallic components is given. The incremental lifetime models provide a promising technique in this context. First of all they rely on the realistic deformation pattern which is computed in the framework of constitutive modeling. Creep, hardening and consequently stress relaxation are properly captured throughout the loading path. Secondly, the underlying lifetime rule can be easy incorporated in the framework as an additional ODE. The engineering handling of the incremental lifetime approach can be thus realized with the available commercial FE tools. The key point is the selection and calibration of an appropriate lifetime rule. This is assumed to be driven by the equivalent viscoplastic rate for a polycrystal component, for instance like in (10), or by the viscoplastic shear strain rates (22) on the slip systems of a single crystal. Doing so, the impact of creep can be quantified following the idea of Danzer, who considers the stationary creep rate as a reference yielding function (13), or applying the linear superposition of creep and fatigue damages (16). The difference in the creep damage under IP and OP TMF conditions is quantified by the phasing factor (15). The lifetime model of type (10) is verified by LCF and TMF tests on Ni-Resist D-5S, demonstrating a very good agreement with the experimental observations.

The conventional incremental time integration of the FE models can possibly result in significant computational efforts. This may be caused by the dimensions, complexity and required fineness of the spacial discretization. However, the dramatical increase in computational costs is much more attributed to those scenarios when lifetime cannot be confidently estimated based on the integration of a limited number of loading cycles, so that the whole fatigue loading history has to be continuously integrated until the onset of failure. Using the accelerated in time computational strategies is advantageous in such situations. The idea behind is to approximate the structural response during the fatigue history based on the integration of a very small number of loading cycles, which is performed at various stages of the structural degradation. The benchmark test demonstrates this idea, where the asymptotic behavior under stress-controlled mode is not achieved because of the impact of damage on deformation. The obtained approximation properly reproduces the stress redistribution within the spacial domain and the damage evolution. The accelerated method was about seven times faster than the respective direct numerical simulation. Notice, an unsaturated viscoplastic response may appear due to ratcheting, even if there is no damage effect on the material stiffness. This can be treated in the similar manner or following the asymptotic expansions of the response fields [72]. Using the accelerated integration schemes are less convenient in application since they require essential implementation efforts. Further, their employing is restricted to lifetime until localization of strain, i.e., initiation of the macroscopic cracks.

Another class of lifetime modeling are the parametric approaches, which are beneficial in view of ease of use. In particular, the fracture mechanics concept is examined in the paper. It is applied to smooth specimens, basically to predict the growth rates of the microcracks when their propagation is the dominant degradation mechanism. The enhanced creep and oxidation at high temperatures can be introduced in the model using (48) and (49). The examples demonstrate reasonable estimations of the lifetimes for variety of mechanical tests on the cast iron Ni-Resist D-5S alloy. The fracture mechanics concept, see Figure 3b, is demonstrated to be much more accurate than the conventional methods based on the plastic strain energy density, see Figure 2. Moreover, the predictive ability was almost comparable with the assessments gained by an incremental model.

An attractive scope of the future research may be development of models and computational concepts for evaluation of interaction between the loadings of different frequencies, including superposition of LCF or TMF with HCF. The first results can be found in the literature, —an extension of the fracture mechanics concept and its application to LCF/HCF is discussed in [77], whereas a TMF/HCF lifetime behavior was recently considered in [78].

Author Contributions: Conceptualization, B.F. and V.K.; Computational Analysis, B.F., V.K. and F.P.; Data Analysis, F.P.; Mechanical Testing, B.R.; Writing—Original Draft Preparation, V.K.; Reviewing and Editing, B.F. and B.R.

Funding: This research was partially funded by the Research Association for Combustion Engines (FVV, Frankfurt) and AG Turbo.

Acknowledgments: The authors thank Jörg F. Unger from BAM in Berlin for useful support concerning FTTI analysis.

Conflicts of Interest: The authors declare no conflict of interest.

Abbreviations

The following abbreviations are used in this manuscript:

LCF	Low-Cycle Fatigue
HCF	High-Cycle Fatigue
TMF	Thermo-Mechanical Fatigue
IP	In Phase
OP	Out Of Phase
ODE	Ordinary Differential Equation
FEM	Finite Element Method
FTTI	Fourier Transformation-Based Integration
WATMUS	WAvelet Transformation MUlti-time Scaling

References

1. Vardar, N.; Ekerim, A. Failure analysis of gas turbine blades in a thermal power plant. *Eng. Fail. Anal.* **2007**, *14*, 743–749. [CrossRef]
2. Williams, J.C.; Starke, E.A. Progress in structural materials for aerospace systems. The Golden Jubilee Issue—Selected topics in Materials Science and Engineering: Past, Present and Future, edited by S. Suresh. *Acta Mater.* **2003**, *51*, 5775–5799. [CrossRef]
3. Kumari, S.; Satyanarayana, D.; Srinivas, M. Failure analysis of gas turbine rotor blades. *Eng. Fail. Anal.* **2014**, *45*, 234–244. [CrossRef]
4. Reed, R. *The Superalloys: Fundamentals and Applications*; Cambridge University Press: Cambridge, UK, 2008.
5. Pineau, A.; Antolovich, S.D. High temperature fatigue: Behaviour of three typical classes of structural materials. *Mater. High Temp.* **2015**, *32*, 298–317. [CrossRef]
6. Sun, Z.; Benabou, L.; Dahoo, P. Prediction of thermo-mechanical fatigue for solder joints in power electronics modules under passive temperature cycling. *Eng. Fract. Mech.* **2013**, *107*, 48–60. [CrossRef]
7. Lee, W.; Nguyen, L.; Selvaduray, G. Solder joint fatigue models: Review and applicability to chip scale packages. *Microelectron. Reliab.* **2000**, *40*, 231–244. [CrossRef]

8. Lee, K.O.; Hong, S.G.; Lee, S.B. A new energy-based fatigue damage parameter in life prediction of high-temperature structural materials. *Mater. Sci. Eng.* **2008**, *496*, 471–477. [CrossRef]
9. Benoit, A.; Maitournam, M.; Rémy, L.; Oger, F. Cyclic behaviour of structures under thermomechanical loadings: Application to exhaust manifolds. *Int. J. Fatigue* **2012**, *38*, 65–74. [CrossRef]
10. Mahtabi, M.J.; Shamsaei, N. A modified energy-based approach for fatigue life prediction of superelastic NiTi in presence of tensile mean strain and stress. *Int. J. Mech. Sci.* **2016**, *117*, 321–333. [CrossRef]
11. Radaj, D.; Sonsino, C.; Fricke, W. *Fatigue Assessment of Welded Joints by Local Approaches*, 2nd ed.; Woodhead Publishing Series in Welding and Other Joining Technologies; Woodhead Publishing: Sawston, UK, 2006. doi:10.1533/9781845691882.433.
12. Lemaitre, J.; Desmorat, R. *Engineering Damage Mechanics: Ductile, Creep, Fatigue and Brittle Failures*; Springer: Berlin/Heidelberg, Germany, 2006.
13. Citarella, R.; Cricrí, G.; Lepore, M.; Perrella, M. Thermo-mechanical Crack Propagation in Aircraft Engine Vane by Coupled FEM-DBEM Approach. *Adv. Eng. Softw.* **2014**, *67*, 57–69. [CrossRef]
14. Fellinger, J.; Citarella, R.; Giannella, V.; Lepore, M.; Sepe, R.; Czerwinski, M.; Herold, F.; Stadler, R. Overview of fatigue life assessment of baffles in Wendelstein 7-X. *Fusion Eng. Des.* **2018**, *136*, 292–297. [CrossRef]
15. Cojocaru, D.; Karlsson, A. A simple numerical method of cycle jumps for cyclically loaded structures. *Int. J. Fatigue* **2006**, *28*, 1677–1689. [CrossRef]
16. Chaboche, J. A review of some plasticity and viscoplasticity constitutive theories. *Int. J. Plast.* **2008**, *24*, 1642–1693. [CrossRef]
17. Méric, L.L.; Poubanne, P.P.; Cailletaud, G.G. Single crystal modeling for structural calculations: Part 1—Model presentation. *J. Eng. Mater. Technol.* **1991**, *113*, 162–170. [CrossRef]
18. Suresh, S. *Fatigue of Materials*, 2nd ed.; Cambridge University Press: Cambridge, UK, 1998. doi:10.1017/CBO9780511806575.
19. Sangid, M.D. The physics of fatigue crack initiation. *Int. J. Fatigue* **2013**, *57*, 58–72. [CrossRef]
20. Calì, C.; Cricrì, G.; Perrella, M. An Advanced Creep Model Allowing for Hardening and Damage Effects. *Strain* **2010**, *46*, 347–357. [CrossRef]
21. Freed, A.D.; Walker, K.P. Viscoplasticity with creep and plasticity bounds. *Int. J. Plast.* **1993**, *9*, 213–242. [CrossRef]
22. McLean, M.; Dyson, B.F. Modeling the effects of damage and microstructural evolution on the creep behavior of engineering alloys. *J. Eng. Mater. Technol.* **2000**, *122*, 273–278. [CrossRef]
23. Frederick, C.; Armstrong, P. A mathematical representation of the multiaxial Bauschinger effect. *Mater. High Temp.* **2007**, *24*, 1–26. [CrossRef]
24. Sermage, J.P.; Lemaitre, J.; Desmorat, R. Multiaxial creep–fatigue under anisothermal conditions. *Fatigue Fract. Eng. Mater. Struct.* **2000**, *23*, 241–252. [CrossRef]
25. Sommitsch, C.; Sievert, R.; Wlanis, T.; Günther, B.; Wieser, V. Modelling of creep-fatigue in containers during aluminium and copper extrusion. *Comput. Mater. Sci.* **2007**, *39*, 55–64. [CrossRef]
26. Sommitsch, C.; Sievert, R.; Wlanis, T.; Redl, C. Lifetime evaluation of two different hot work tool steels in aluminium extrusion. *Comput. Mater. Sci.* **2008**, *43*, 82–91. [CrossRef]
27. Satoh, M.; Kremp, E. An incremental life prediction law for creep–fatigue interaction. In *Material Behaviour at Elevated Temperatures and Components Analysis*; Yamada, Y., Cho, F., Roche, R., Eds.; American Society of Mechanical Engineers PVP: New York, NY, USA, 1982; Volume 10, pp. 71–79.
28. Yeh, N.; Kremp, E. An incremental life prediction law for multiaxial creep-fatigue interaction and thermomechanical loading. In *Advances in Multiaxial Fatigue*; McDowell, D., Ellis, R., Eds.; American Society for Testing and Materials STP 1191; ASTM International: West Conshohocken, PA, USA, 1993; pp. 107–119.
29. Majumdar, S.; Maiya, P. A mechanistic model for time-dependent fatigue. *J. Eng. Mater. Technol.* **1980**, *102*, 159–167. [CrossRef]
30. Majumdar, S. Designing against low-cycle fatigue at elevated temperature. *Nucl. Eng. Des.* **1981**, *63*, 121–135. [CrossRef]
31. Brown, M.W.; Miller, K.J. A theory for fatigue failure under multiaxial stress-strain conditions. *Proc. Inst. Mech. Eng.* **1973**, *187*, 745–755. [CrossRef]

32. Robinson, E.L. Effect of temperature variation on the long-time rupture strength of steels. *Trans. Am. Soc. Mech. Eng.* **1952**, *74*, 777–780.
33. Danzer, R.; Bressers, J. A new method to predict the life under high-temperature low cycle fatigue conditions. *Fatigue Fract. Eng. Mater. Struct.* **1986**, *9*, 151–168. [CrossRef]
34. Franklin, C. Cyclic creep and fatigue life time prediction. In *High Temperature Alloys for Gas Turbines*; Coutsouradis, D., Felix, P., Fischmeister, H., Habraken, L., Lindblom, Y., Speidel, M.O., Eds.; Applied Science: London, UK, 1978; pp. 513–547.
35. Rémy, L.; Rezai-Aria, F.; Danzer, R.; Hoffelner, W. Evaluation of life prediction methods in high temperature fatigue. In *Low Cycle Fatigue*; Solomon, H.D., Halford, G.R., Kaisand, L.R., Leis, B.N., Eds.; American Society for Testing and Materials STP 942; ASTM International: West Conshohocken, PA, USA, 1988; pp. 1115–1132.
36. Vöse, F.; Becker, M.; Fischersworring-Bunk, A.; Hackenberg, H.P. An approach to life prediction for a nickel-base superalloy under isothermal and thermo-mechanical loading conditions. *Int. J. Fatigue* **2013**, *53*, 49–57. [CrossRef]
37. Inoue, T.; Okazaki, M.; Igari, T.; Sakane, M.; Kishi, S. Evaluation of fatigue-creep life prediction methods in multiaxial stress state: The second report of the benchmark project (B) by the Subcommittee on Inelastic Analysis and Life Prediction of High Temperature Materials, JSMS. *Nucl. Eng. Des.* **1991**, *126*, 13–21. [CrossRef]
38. Tinga, T.; Brekelmans, W.; Geers, M. Time-incremental creep–fatigue damage rule for single crystal Ni-base superalloys. *Mater. Sci. Eng.* **2009**, *508*, 200–208. [CrossRef]
39. Charles, C.M.; Drew, G.A.; Bagnall, S.; Rae, C.M. Dislocation deformation mechanisms during fatigue of the nickel-based superalloy CMSX-4. In *Materials Science Forum*; Progress in Light Metals, Aerospace Materials and Superconductors; Trans Tech Publications: Zurich, Switzerland, 2007; Volume 546, pp. 1211–1218. doi:10.4028/www.scientific.net/MSF.546-549.1211.
40. Chan, K.S.; Hack, J.E.; Leverant, G.R. Fatigue crack growth in MAR-M200 single crystals. *Metall. Mater. Trans.* **1987**, *18*, 581–591. [CrossRef]
41. Telesman, J.; Ghosn, L.J. Fatigue crack growth behavior of PWA 1484 single crystal superalloy at elevated temperatures. *J. Eng. Gas Turbines Power* **1996**, *118*, 399–405. [CrossRef]
42. Kagawa, H.; Mukai, Y. The effect of crystal orientation and temperature on fatigue crack growth of Ni-based single crystal superalloy. In *Superalloys 2012*; Wiley-Blackwell: Hoboken, NJ, USA, 2012; pp. 225–233, doi:10.1002/9781118516430.ch25.
43. MacLachlan, D.W.; Knowles, D.M. Fatigue behaviour and lifing of two single crystal superalloys. *Fatigue Fract. Eng. Mater. Struct.* **2011**, *24*, 503–521. [CrossRef]
44. Hong, H.U.; Choi, B.G.; Kim, I.S.; Yoo, Y.S.; Jo, C.Y. Characterization of deformation mechanisms during low cycle fatigue of a single crystal nickel-based superalloy. *J. Mater. Sci.* **2011**, *46*, 5245–5251. [CrossRef]
45. Chen, Q.; Liu, H.W. Resolved shear stress intensity coefficient and fatigue crack growth in large crystals. *Theor. Appl. Fract. Mech.* **1988**, *10*, 111–122. [CrossRef]
46. Qiu, W.; Ma, X.; Rui, S.; Shi, H.J. Crystallographic analysis on small fatigue crack propagation behaviour of a nickel-based single crystal superalloy. *Fatigue Fract. Eng. Mater. Struct.* **2016**, *40*, 3–11. [CrossRef]
47. Levkovitch, V.; Sievert, R.; Svendsen, B. Simulation of deformation and lifetime behavior of a fcc single crystal superalloy at high temperature under low-cycle fatigue loading. *Int. J. Fatigue* **2006**, *28*, 1791–1802. [CrossRef]
48. Staroselsky, A.; Cassenti, B.N. Creep, plasticity, and fatigue of single crystal superalloy. *Int. J. Solids Struct.* **2011**, *48*, 2060–2075. [CrossRef]
49. Antolovich, S.D.; Liu, S.; Baur, R. Low cycle fatigue behavior of René 80 at elevated temperature. *Metall. Trans.* **1981**, *12*, 473–481. [CrossRef]
50. Reuchet, J.; Remy, L. Fatigue oxidation interaction in a superalloy—Application to life prediction in high temperature low cycle fatigue. *Metall. Trans.* **1983**, *14*, 141–149. [CrossRef]
51. Neu, R.W.; Sehitoglu, H. Thermomechanical fatigue, oxidation, and creep: Part II—Life prediction. *Metall. Trans. A* **1989**, *20A*, 1769–1783. [CrossRef]
52. Neumann, P. The geometry of slip processes at a propagating fatigue crack-II. *Acta Metall.* **1974**, *22*, 1167–1178. [CrossRef]

53. Gross, D.; Seelig, T. *Fracture Mechanics: With an Introduction to Micromechanics*; Mechanical Engineering Series; Springer: Berlin/Heidelberg, Germany, 2011.
54. Shih, C.F. Relationships between the J-integral and the crack opening displacement for stationary and extending cracks. *J. Mech. Phys. Solids* **1981**, *29*, 305–326. [CrossRef]
55. Schmitt, W.; Mohrmann, R.; Riedel, H.; Dietsche, A.; Fischersworring-Bunk, A. Modelling of the fatigue life of automobile exhaust components. In Proceedings of the 8th International Fatigue Congress, Stockholm, Sweden, 3–7 June 2002; Blom, A., Ed.; Engineering Materials Advisory Services: Stockholm, Sweden, 2002; Volume 2, pp. 781–788.
56. Heitmann, H.; Vehoff, H.; Neumann, P. Life prediction for random load fatigue based on the growth behavior of microcracks. In *Fracture 84*; Valluri, S., Taplin, D., Rama Rao, P., Knott, J., Dubey, R., Eds.; Pergamon Press: Oxford, UK, 1984; pp. 3599–3606. doi:10.1016/B978-1-4832-8440-8.50388-4.
57. Vormwald, M.; Seeger, T. The consequences of short crack closure on fatigue crack growth under variable amplitude loading. *Fatigue Fract. Eng. Mater. Struct.* **1991**, *14*, 205–225. [CrossRef]
58. Schijve, J. Some formulas for the crack opening stress level. *Eng. Fract. Mech.* **1981**, *14*, 461–465. [CrossRef]
59. Newman, J.C. A crack opening stress equation for fatigue crack growth. *Int. J. Fract.* **1984**, *24*, R131–R135. [CrossRef]
60. Pippan, R.; Hohenwarter, A. Fatigue crack closure: A review of the physical phenomena. *Fatigue Fract. Eng. Mater. Struct.* **2017**, *40*, 471–495. [CrossRef]
61. Gruetzner, S.; Fedelich, B.; Rehmer, B.; Buchholz, B. Material modelling and lifetime prediction of Ni-Base gas turbine blades under TMF conditions. In *Advanced Materials Research*; Trans Tech Publications: Zurich, Switzerland, 2014; Volume 891, pp. 1277–1282. doi:10.4028/www.scientific.net/AMR.891-892.1277.
62. Riedel, H. *Fracture at High Temperatures*; Materials Research and Engineering; Springer: Berlin/Heidelberg, Germany, 1987.
63. Miller, M.P.; McDowell, D.L.; Oehmke, R.L.T. A creep-fatigue-oxidation microcrack propagation model for thermomechanical fatigue. *J. Eng. Mater. Technol.* **1992**, *114*, 282–288. [CrossRef]
64. Christ, H.J. Effect of environment on thermomechanical fatigue life. *Mater. Sci. Eng. A* **2007**, *468–470*, 98–108. [CrossRef]
65. Vöse, F.; Becker, M.; Fischersworring-Bunk, A.; Hackenberg, H.P. A mechanism-based approach to life prediction for a nickel-base alloy subjected to cyclic and creep-fatigue. *Tech. Mech.* **2012**, *32*, 595–607.
66. Metzger, M.; Nieweg, B.; Schweizer, C.; Seifert, T. Lifetime prediction of cast iron materials under combined thermomechanical fatigue and high cycle fatigue loading using a mechanism-based model. *Int. J. Fatigue* **2013**, *53*, 58–66. [CrossRef]
67. Kühn, H.J.; Rehmer, B.; Skrotzki, B. Thermomechanical fatigue of heat-resistant austenitic cast iron EN-GJSA-XNiSiCr35-5-2 (Ni-Resist D-5S). *Int. J. Fatigue* **2017**, *99*, 295–302. [CrossRef]
68. Maitournam, H.; Pommier, B.; Comte, F.; Nguyen-Tajan, T.M.L. Direct cyclic methods for structures under thermomechanical loading. In Proceedings of the European Conference on Computational Mechanics (ECCM 2010), Paris, France, 16–21 May 2010.
69. Spiliopoulos, K.V.; Panagiotou, K.D. A direct method to predict cyclic steady states of elastoplastic structures. *Comput. Methods Appl. Mech. Eng.* **2012**, *223–224*, 186–198. [CrossRef]
70. Fish, J.; Bailakanavar, M.; Powers, L.; Cook, T. Multiscale fatigue life prediction model for heterogeneous materials. *Int. J. Numer. Methods Eng.* **2012**, *91*, 1087–1104. [CrossRef]
71. Crouch, R.; Oskay, C. Accelerated time integrator for multiple time scale homogenization. *Int. J. Numer. Methods Eng.* **2015**, *101*, 1019–1042. [CrossRef]
72. Haouala, S.; Doghri, I. Modeling and algorithms for two-scale time homogenization of viscoelastic-viscoplastic solids under large numbers of cycles. *Int. J. Plast.* **2015**, *70*, 98–125. [CrossRef]
73. Kindrachuk, V.M.; Unger, J.F. A Fourier transformation-based temporal integration scheme for viscoplastic solids subjected to fatigue deterioration. *Int. J. Fatigue* **2017**, *100*, 215–228. [CrossRef]
74. Kindrachuk, V.M.; Titscher, T.; Unger, J.F. A Fourier transformation-based method for gradient-enhanced modeling of fatigue. *Int. J. Numer. Methods Eng.* **2018**, *114*, 196–214. [CrossRef]
75. Chakraborty, P.; Ghosh, S. Accelerating cyclic plasticity simulations using an adaptive wavelet transformation based multitime scaling method. *Int. J. Numer. Methods Eng.* **2013**, *93*, 1425–1454. [CrossRef]

76. Yaghmaie, R.; Guo, S.; Ghosh, S. Wavelet transformation-induced multi-time scaling (WATMUS) model for coupled transient electro-magnetic and structural dynamics finite element analysis. *Comput. Methods Appl. Mech. Eng.* **2016**, *303*, 341–373. [CrossRef]
77. Schweizer, C.; Seifert, T.; Nieweg, B.; von Hartrott, P.; Riedel, H. Mechanisms and modelling of fatigue crack growth under combined low and high cycle fatigue loading. *Int. J. Fatigue* **2011**, *33*, 194–202. [CrossRef]
78. Fedelich, B.; Kühn, H.J.; Rehmer, B.; Skrotzki, B. Experimental and analytical investigation of the TMF-HCF lifetime behavior of two cast iron alloys. *Int. J. Fatigue* **2017**, *99*, 266–278. [CrossRef]